Electro-optic and nonlinear optical properties of ion implanted waveguides in organic crystals

Lukas Mutter,* Mojca Jazbinšek, Christian Herzog, and Peter Günter

Nonlinear Optics Laboratory, Institute of Quantum Electronics, ETH Zurich, CH-8093 Zurich, Switzerland

nlo@phys.ethz.ch

Abstract: We report on the electro-optic and nonlinear optical properties of waveguides produced by low fluence ($\phi = 1.25 \times 10^{14}$ ions/cm^2) H^+ ion implantation in the organic nonlinear optic crystal 4-N, N-dimethylamino-4'-N'-methyl-stilbazolium tosylate (DAST). The profile of the nonlinear optical susceptibility has been determined by measuring the reflected second-harmonic generation efficiency from a wedged-polished sample at a fundamental wavelength of $\lambda_\omega = 1176$nm. In the waveguide core region the nonlinear optical susceptibility is shown to be preserved to more than 90% of its bulk value. A model which relates the molecular changes to the measured macroscopic alteration of the refractive index and the nonlinear coefficient has been introduced to quantify the fraction of molecules modified by ion implantation. Furthermore, a first electro-optic modulation in ion implanted DAST waveguides has been demonstrated.

© 2008 Optical Society of America

OCIS codes: (230.7390) Waveguides, planar; (230.2090) Electro-optical devices; (190.4350) Nonlinear optics at surfaces

References and links

1. Y. Enami, C.T. Derose, D. Mathine, C. Loychik, C. Greenlee, R. A. Norwood, T.D. Kim, J. Luo, Y. Tian, A. K. Y. Jen and N. Peyghambarian, "Hybrid polymer/so-gel waveguide modulators with exceptionally large electro-optic coefficients," Nature Photonics **1** (3), 180-185 (2007).
2. M. Hochberg, T. Baehr-Jones, G. X. Wang, M. Shearn, K. Harvard, J. D. Luo, B. Q. Chen, Z. W. Shi, R. Lawson, P. Sullivan, A. K. Y. Jen, L. Dalton, and A. Scherer, "Terahertz all-optical modulation in a silicon-polymer hybrid system," Nat. Mater. **5**, 703-709 (2006).
3. T. Kaino, B. Cai, and K. Takayama, "Fabrication of DAST channel optical waveguides," Adv. Funct. Mater. **12**, 599-603 (2002).
4. W. Geis, R. Sinta, W. Mowers, S. J. Deneault, M. F. Marchant, K. E. Krohn, S. J. Spector, D. R. Calawa, and T. M. Lyszczarz, "Fabrication of crystalline organic waveguides with an exceptionally large electro-optic coefficient," Appl. Phys. Lett. **84**, 3729-3731 (2004).
5. L. Mutter, M. Koechlin, M. Jazbinšek, and P. Günter, "Direct electron beam writing of channel waveguides in nonlinear optical organic crystals," Opt. Express **15**, 16828-16838 (2007).
6. U. Meier, M. Bösch, Ch. Bosshard, F. Pan, and P. Günter, "Parametric interactions in the organic salt 4-N, N-dimethylamino-4'-N'-methyl-stilbazolium tosylate at telecommunication wavelengths," J. Appl. Phys. **83**, 3486-3489 (1998).
7. F. Pan, G. Knöpfle, Ch. Bosshard, S. Follonier, R. Spreiter, M. S. Wong, and P. Günter, "Electro-optic properties of the organic salt 4-N, N-dimethylamino-4'-N'-methyl-stilbazolium tosylate," Appl. Phys. Lett. **69**, 13-15 (1996).
8. P. D. Townsend, P. J. Chandler, and L. Zhang, *Optical effects of ion implantation*, (Cambridge U. Press, 1994).
9. P. D. Townsend, "Development of ion implantation for optical applications," Vacuum **51**, 301-304 (1998).

#90071 - $15.00 USD Received 27 Nov 2007; revised 4 Jan 2008; accepted 4 Jan 2008; published 9 Jan 2008

10. L. Mutter, A. Guarino, M. Jazbinšek, M. Zgonik, and P. Günter, "Ion implanted optical waveguides in nonlinear optical organic crystal," Opt. Express **15**, 629-638 (2007).
11. D. Fluck, T. Pliska, M. Küpfer, and P. Günter, "Depth profile of the nonlinear optical susceptibility of ion-implanted $KNbO_3$ waveguides," Appl. Phys. Lett. **67**, 748-750 (1995).
12. J. Olivares, A. Garcia-Navarro, G. Garcia, A. Mendez, F. Agullo-Lopez, A. Garcia-Cabanes, M. Carrascosa, and O. Caballero, "Nonlinear optical waveguides generated in lithium niobate by swift-ion irradiation at ultralow fluences," Opt. Lett. **32**, 2587-2589 (2007).
13. F. Pan, M. S. Wong, Ch. Bosshard, and P. Günter, "Crystal growth and characterization of the organic salt 4-N, N-dimethylamino-4'-N'-methyl-stilbazolium tosylate (DAST)," Adv. Mater. **8**, 592-595 (1996).
14. L. Mutter, M. Jazbinšek, M. Zgonik, U. Meier, Ch. Bosshard, P. and Günter, "Photobleaching and optical properties of organic crystal 4-N, N-dimethylamino-4'-N'-methyl-stilbazolium tosylate," J. Appl. Phys. **94**, 1356-1361 (2003).
15. A. Guarino, P. Günter, "Nondestructive method for the characterization of ion-implanted waveguides," Opt. Lett. **30**, 2412-2414 (2005).
16. M. R. Ramadas, E. Garmire, A. K. Ghatak, K. Thyagarajan, and M. R. Shenoy, "Analysis of absorbing and leaky planar waveguides: a novel method," Opt. Lett. **14**, 376-378 (1989).
17. N. Bloembergen, P. S. Pershan, "Light waves at the boundary of nonlinear media," Phys. Rev. **128**, 606-622 (1962).
18. Ch. Bosshard, K. Sutter, Ph. Prêtre, J. Hulliger, M. Flörsheimer, P. Kaatz, and P. Günter, *Organic nonlinar optical materials*, (Gordon and Breach Science Publishers SA, 1995).

1. Introduction

Organic nonlinear optical materials offer numerous design possibilities and generally exhibit higher and faster nonlinearities compared to their inorganic counterparts [1, 2]. While poled electro-optic polymers are easier to process, organic crystals show superior thermal stability, but the realization of waveguides is still challenging [3, 4, 5].

DAST (4-N, N-dimethylamino-4'-N'-methyl-stilbazolium tosylate) is an organic crystal with outstanding nonlinear optical properties, e.g. a second-order nonlinear optical coefficient $(d = \chi^{(2)}/2)$ $d_{111} = 1010 \pm 110$ pm/V at a fundamental wavelength of 1318 nm, and $d_{111} = 210 \pm 55$ pm/V at 1907 nm [6]. Furthermore, the combination of a low dielectric constant of $\varepsilon_{11} = 5.2$ with a high electro-optic figure of merit, $n_1^3 r_{111} = 1030 \pm 110$ pm/V at 800 nm and $n_1^3 r_{111} = 455 \pm 80$ pm/V at 1535 nm, are rendering it highly attractive for high-speed electro-optic applications [7].

Ion implantation is used in a variety of inorganic materials to produce optical waveguide structures [8, 9]. Recently, it has also been applied to the organic nonlinear optical crystal DAST, in which planar optical waveguides have been successfully realized by light ion implantation [10]. A barrier layer with a reduced index of refraction was formed a few micrometers below the surface by low fluence irradiation of 1 MeV H^+ ions, and thus confinement of light was ensured in the core layer between sample surface and barrier.

To use ion implanted waveguides for active integrated photonic devices, it is of main importance to maintain the high nonlinear optical properties in the waveguide region. In inorganic nonlinear optical active crystals such as $KNbO_3$ or $LiNbO_3$, a reduction of the nonlinear optical properties below 50% of its bulk value was observed upon implantation [11, 12]. With thermal annealing and subsequent repoling the optical nonlinearity was recovered to more than 90% of the bulk value [11]. In organic nonlinear optical crystals, the origins of the refractive index change by ion implantation are electronic excitations [10], and are therefore essentially different compared to inorganic crystals, in which the refractive index changes are due to ion induced nuclear displacements. The influence of ion implantation on the nonlinear optical properties of organic crystals has not been investigated yet.

In this work we present our results on the measured nonlinear optical susceptibility profile of H^+ implanted waveguides in DAST. We introduce a model that relates microscopic material changes to the observed alteration of the nonlinear optical susceptibility. Furthermore, we report on the first electro-optic modulation experiments in the produced waveguide structures.

#90071 - $15.00 USD Received 27 Nov 2007; revised 4 Jan 2008; accepted 4 Jan 2008; published 9 Jan 2008
(C) 2008 OSA

2. Ion implanted waveguides in DAST

The DAST single crystals used in our experiments were grown from supersaturated methanol solution by the temperature-lowering method [13]. DAST has a monoclinic point-group symmetry *m* with its mirror plane normal to the *b* axis. The crystallographic x_1 and x_3 axes coincide almost with the crystallographic *a* and *c* axis, respectively [14]. The grown crystals were cut approximately along the dielectric axes and the x_1x_2 surface was polished to $\lambda/4$ quality. The typical sample size was about $7 \times 4 \times 4\,\mathrm{mm}^3$ with the longest dimension along x_1.

The x_1x_2 sample surface was then irradiated with 1 MeV H^+ ions with a fluence of $\phi = 1.25 \times 10^{14}\,\mathrm{ions/cm}^2$. In order to reduce the penetration depth of the ions, the samples were tilted by 60° from normal incidence, resulting in an induced refractive index barrier at a depth of about $9\,\mu$m. The ion current was kept at 40 nA and scanned over an area of $9 \times 9\,\mathrm{mm}^2$ to avoid thermal damage to the samples.

We have previously shown that using these implantation parameters a refractive index barrier suitable for waveguiding is formed with a peak refractive index change of $\Delta n_1 = -0.1$ at a probing wavelength of 810 nm [10]. The refractive index profile at this wavelength was measured by detecting the reflected light from a wedged-polished sample surface and the corresponding effective mode indices were determined by the barrier coupling method [15]. By conventional end-fire coupling waveguiding at telecommunication wavelength was demonstrated with measured waveguide losses of about 7 dB/cm.

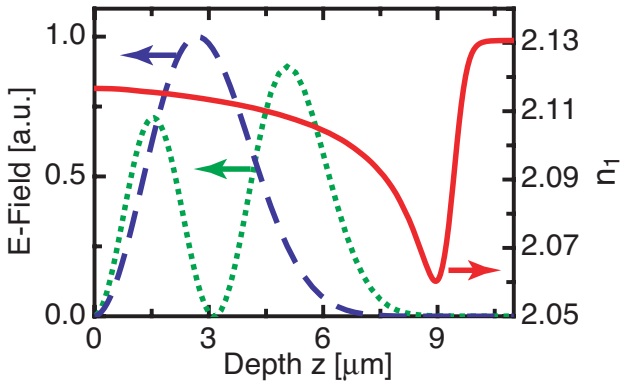

Fig. 1. Refractive index profile of ion implanted DAST waveguides at a wavelength of $1.55\,\mu$m (solid curve) for an ion fluence of $\phi = 1.25 \times 10^{14}\,\mathrm{ions/cm}^2$, and corresponding optical field amplitude of the first (dashed curve) and second mode (dotted curve), which have calculated tunneling losses of below 1 dB/cm.

The study of the fundamental waveguide properties at $\lambda = 1.55\,\mu$m (refractive index as well as waveguide mode profiles) is of significant importance concerning the use of DAST for high-speed optical modulators and switches in telecommunication.

With help of the previously obtained refractive index data at 810 nm [10] and the model described in detail in Section 4.1, the refractive index profile at a wavelength of $1.55\,\mu$m was obtained. Figure 1 shows the refractive index profile with the corresponding optical field distributions of the first and second TE mode, whose effective indices were calculated to be $n_{\mathrm{eff},1} = 2.111$ and $n_{\mathrm{eff},2} = 2.102$, respectively, by using a 2×2 matrix formalism [8]. The tunneling losses were determined with help of the width of the resonance peaks obtained by the matrix formalism [16] and are below 1 dB/cm for the modes depicted. Higher order modes show tunneling loss estimates of over 10 dB/cm. Therefore the produced waveguide can be considered to be bimodal.

#90071 - $15.00 USD Received 27 Nov 2007; revised 4 Jan 2008; accepted 4 Jan 2008; published 9 Jan 2008
(C) 2008 OSA

3. Second-harmonic reflection measurement

In order to determine the change of the nonlinear optical susceptibility as a function of the implantation depth, the reflected second-harmonic generated light from a wedged-polished sample surface was measured. To increase the resolution of the measurement, the sample was polished under an angle of 1° as shown in Fig. 2. The output of an optical parametric generator/amplifier OPG/OPA (Quantronix, TOPAS), which was pumped with a Ti:sapphire laser providing 160 fs pulses at a center wavelength of 776 nm with a repetition rate of 1 kHz, was then focused on the sample surface to a diameter of less than 10 μm. The sample was scanned in η direction with a step size of 10 μm leading to a depth resolution of about 0.2 μm in z direction. Signal distortions due to polishing imperfections were reduced by averaging over 19 scans taken at different positions. A fundamental wavelength of $\lambda_\omega = 1176$ nm was chosen so that the second-harmonic generated light at $\lambda_{2\omega} = 588$ nm was within the visible absorption band of DAST [14]. Therefore, only the second-harmonic generated light at the sample surface was observed and any substrate contributions were eliminated [11]. The polarization of the fundamental beam was parallel to the x_1 direction.

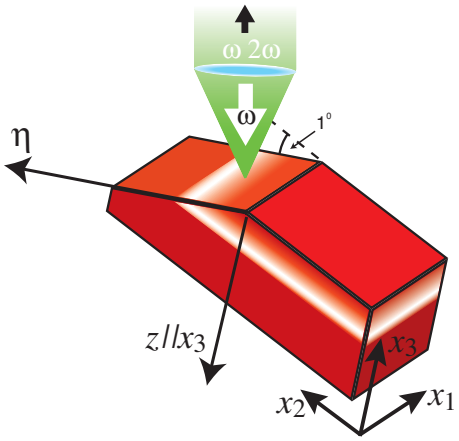

Fig. 2. Experimental setup for measuring the depth profile of the nonlinear optical susceptibility. The second-harmonic light generated on a wedged sample surface is measured while the sample is scanned in η direction. The profile as a function of the implantation depth z is finally obtained by a projection of the η to the z direction.

A light beam impinging on an interface between a linear and a nonlinear optical active medium will result in a second-harmonic reflected wave. For normal incidence the existence of a second-harmonic reflected wave can be explained with the boundary conditions that require continuous tangential electric and magnetic field components. Since in the nonlinear medium waves with second-harmonic frequency exist, the boundary condition can only be fulfilled with the presence of a back reflected second-harmonic wave. For normal incidence the second-harmonic reflected field component $E^R_{2\omega}$ at an interface between a linear and a nonlinear optical active medium is related to the induced nonlinear polarizability $P^{\mathrm{NLS}}_{2\omega}$ in the active medium by [17]

$$E^R_{2\omega} = \frac{1}{\varepsilon_0}\frac{P^{\mathrm{NLS}}_{2\omega}}{(n_{2\omega}+1)(n_{2\omega}+n_\omega)} = \frac{d_{111}t^2_\omega E^2_\omega}{(n_{2\omega}+1)(n_{2\omega}+n_\omega)}, \tag{1}$$

where n_ω and $n_{2\omega}$ are the refractive indices along the x_1 axis of DAST at the fundamental and second-harmonic frequencies, respectively. E_ω is the incident electric field in air, $t_\omega =$

#90071 - $15.00 USD Received 27 Nov 2007; revised 4 Jan 2008; accepted 4 Jan 2008; published 9 Jan 2008
(C) 2008 OSA

$2/(n_\omega+1)$ the transmission factor for the electric field amplitude E_ω, d_{111} the tensor element of the nonlinear optical susceptibility tensor $d_{ijk}=\frac{1}{2}\chi^{(2)}_{ijk}$, and ε_0 the dielectric permittivity of free space. The back reflected light was deflected on a beamsplitter and measured with a photo avalanche diode. We ensured that only the second-harmonic intensity was detected by inserting a band pass and an interference filter, which were blocking the fundamental beam, in the beam path between the beamsplitter and the photodiode.

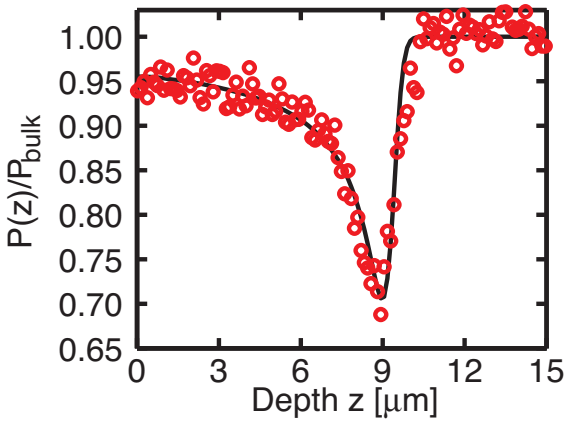

Fig. 3. Measured normalized second-harmonic power of an implanted DAST waveguide as a function of the implantation depth z at a second-harmonic wavelength of $\lambda_{2\omega}=588\,\mathrm{nm}$. The open circles represent the measured data points. The full curve is a guide to the eye.

The measured second-harmonic generated power as a function of the depth z normalized by its bulk value is shown in Fig. 3. In the waveguide core region a reduction of the normalized power of less than 10% was present, whereas within the barrier layer the signal dropped to about 70% of the bulk value of the virgin crystal.

4. Ion-induced modification of linear and nonlinear optical properties in organic media

4.1. Model

Since the quantity of interest is the change of the nonlinear optical susceptibility after implantation, we introduce a model which relates the microscopic and macroscopic properties to the measured second-harmonic power. With help of this model the nonlinear susceptibility d_{ijk} as well as the number of modified molecules will be calculated.

The microscopic linear polarizability $\alpha(\omega)$ at frequency ω and the first-order hyperpolarizability $\beta(-2\omega,\omega,\omega)$ at the fundamental frequency ω are related to the refractive index n and nonlinear susceptibility d by [18]

$$n_\omega^2-1=N f_\omega \alpha(\omega) \tag{2}$$

$$d=\frac{1}{2}N f_\omega^2 f_{2\omega}\beta(-2\omega,\omega,\omega), \tag{3}$$

where N is the number of molecules per volume and $f_{\omega,2\omega}=(n^2_{\omega,2\omega}+2)/3$ are Lorentz local field factors.

After implantation, some nonlinear optical chromophores of the implanted DAST crystals will be modified. This leads to a reduction of the molecular polarizability α and the first-order

#90071 - $15.00 USD Received 27 Nov 2007; revised 4 Jan 2008; accepted 4 Jan 2008; published 9 Jan 2008
(C) 2008 OSA

hyperpolarizability β and hence to an alteration of the macroscopic material properties n and d. The polarizability $\tilde{\alpha}$ of the modified molecules can be described by

$$\tilde{\alpha}(\omega) = k_\omega \alpha(\omega), \tag{4}$$

where k_ω is the fraction of remaining polarizability of the modified molecule. If we assume that the first order hyperpolarizability of the modified molecules $\tilde{\beta}$ is

$$\tilde{\beta}(-2\omega,\omega,\omega) << \beta(-2\omega,\omega,\omega), \tag{5}$$

we obtain for the refractive index $\tilde{n}_\omega(z)$ and the nonlinear susceptibility $\tilde{d}(z)$ of the implanted material

$$\tilde{n}_\omega^2(z) - 1 = Np(z)\tilde{f}_\omega(z)\alpha(\omega) + N[1-p(z)]\tilde{f}_\omega(z)\tilde{\alpha}(\omega) \tag{6}$$

$$\tilde{d}(z) \approx \frac{1}{2} Np(z)\tilde{f}_\omega^2(z)\tilde{f}_{2\omega}(z)\beta(-2\omega,\omega,\omega), \tag{7}$$

where $p(z)$ is the fraction of unmodified chromophores at the depth z. Dividing Eq. (7) by Eq. (3), we obtain for the fraction of unmodified molecules

$$p(z) = \frac{\tilde{d}(z)}{d_{\text{bulk}}} \frac{f_\omega^2 f_{2\omega}}{\tilde{f}_\omega^2(z)\tilde{f}_{2\omega}(z)}. \tag{8}$$

With help of Eq. (1) the following relation can be derived for the normalized susceptibility profile $\tilde{d}(z)/d_{\text{bulk}}$

$$\frac{\tilde{d}(z)}{d_{\text{bulk}}} = \sqrt{\frac{P(z)}{P_{\text{bulk}}}} \frac{[\tilde{n}_{2\omega}(z)+1][\tilde{n}_{2\omega}(z)+\tilde{n}_\omega(z)]}{[n_{2\omega}+1][n_{2\omega}+n_\omega]} \frac{t_\omega^2}{\tilde{t}_\omega^2(z)}, \tag{9}$$

where $P(z)/P_{\text{bulk}}$ is the measured normalized power depicted in Fig. 3. Therefore, if the refractive index profiles $\tilde{n}_{2\omega}(z)$ and $\tilde{n}_\omega(z)$ are known, the normalized susceptibility profile $\tilde{d}(z)/d_{\text{bulk}}$ can be calculated. Subsequently also the fraction of unmodified molecules $p(z)$ given by Eq. (8) can be determined, since the local field factors are only dependent on the refractive index profile data.

4.2. Susceptibility profile

The refractive index profiles for our implantation parametes at a wavelength of 633 nm and 810 nm are given in Ref.[10] . The one at 633 nm was extrapolated to the wavelength of the second-harmonic light at 588 nm and the profile at 810 nm was used to obtain the corresponding refractive index profile data at the fundamental wavelength of 1176 nm with the following procedure.

With help of Eqs. (2), (4) and (6), $p(z)$ can be written as

$$p(z) = \frac{\frac{\tilde{n}_\omega^2(z)-1}{\tilde{n}_\omega^2(z)+2}\frac{n_\omega^2+2}{n_\omega^2-1} - k_\omega}{1-k_\omega}. \tag{10}$$

Since the fraction of unmodified molecules $p(z)$ is independent of the wavelength, the refractive index profile $\tilde{n}_{\omega'}(z)$ at the frequency ω' can be calculated with help of the following equation

$$\frac{\frac{\tilde{n}_\omega^2(z)-1}{\tilde{n}_\omega^2(z)+2}\frac{n_\omega^2+2}{n_\omega^2-1} - k_\omega}{1-k_\omega} = \frac{\frac{\tilde{n}_{\omega'}^2(z)-1}{\tilde{n}_{\omega'}^2(z)+2}\frac{n_{\omega'}^2+2}{n_{\omega'}^2-1} - k_{\omega'}}{1-k_{\omega'}}. \tag{11}$$

#90071 - $15.00 USD Received 27 Nov 2007; revised 4 Jan 2008; accepted 4 Jan 2008; published 9 Jan 2008
(C) 2008 OSA

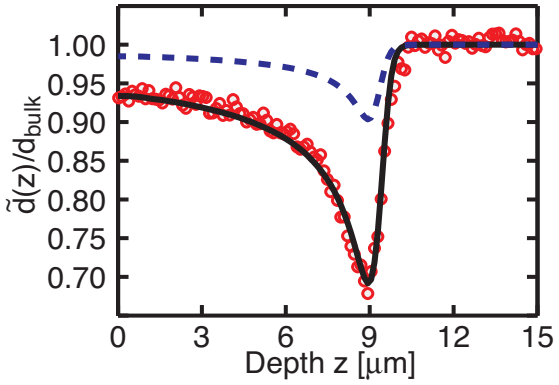

Fig. 4. Open circles represent the normalized susceptibility profile of a waveguide structure produced by 1 MeV H^+ implantation with a fluence of $\phi = 1.25 \times 10^{14}$ ions/cm^2. The full curve corresponds best the theoretical model based on Eq. (12). The dashed curve is the fraction of unmodified molecules calculated with Eq. (8).

Assuming that $k_\omega \approx k_{\omega'}$, the refractive index profiles $\tilde{n}_\omega(z)$ and $\tilde{n}_{2\omega}(z)$ were calculated with help of the refractive index data at 633 nm and 810 nm and the reported bulk refractive indices of $n_\omega = 2.18$ at 1176 nm [7] and $n_{2\omega} = 3.10$ at a wavelength of 588 nm [14].

Figure 4 shows the normalized susceptibility profile (open circles) obtained from the measured $P(z)/P_{\text{bulk}}$ data using Eq. (9). Note the similarity of the amplitudes of the normalized measured power (Fig. 3) to the one of the susceptibility profile (Fig. 4). As substantiated in Eq. (9), the normalized susceptibility profile is proportional to the square root of the normalized measured power. Taking also into account the reduction of the refractive index in the implanted region, which is usually neglected when analyzing induced waveguides, we obtained the described amplitude similarity. The fraction of unmodified molecules $p(z)$ is represented by a dashed curve as calculated with Eq. (8). At the peak position about 10% of the molecules were modified. At the position of the maximal optical field of the first mode (see Fig. 1), about 2% of the molecules were modified, which decreased the nonlinear optical susceptibility by about 6%.

To describe the nonlinear susceptibility profile as a function of the deposited energy, we have chosen a model analogous to the one used for the refractive index change, in which the deposited energy was related to the induced refractive index change [10]. Hence, the relative change in the nonlinear susceptibility is given by

$$\frac{\Delta\tilde{d}(z)}{d_{\text{bulk}}} = \frac{\Delta d_{\max}}{d_{\text{bulk}}}\left[1 - e^{-\left(\phi\frac{G_{el}(\mu z)}{G_{el,0}}\right)^{\gamma_{el}}}\right], \tag{12}$$

where $\Delta d_{\max}$ is the maximal change in d. $G_{el,0}$ is a normalization energy term and γ_{el} is an exponential factor. G_{el} represents the deposited energy as calculated with Srim [10] and the factor μ accounts for the limited precision in the prediction of the ion range by Srim. The full curve in Fig. 4 corresponds best to the experimental data obtained by least-squares theoretical analysis. The obtained parameters are summarized in Table 1 with the following remarks. For the analysis, $\Delta d_{\max}/d_{\text{bulk}}$ was fixed to -1, since (i) for very high fluences all molecules should be modified and therefore the second-order nonlinear activity of the material lost, and (ii) we are in a low fluence regime as mentioned in Ref. [10], therefore the parameters $G_{el,0}$ and $\Delta d_{\max}/d_{\text{bulk}}$ are not independent from each other. Moreover, the factor μ was fixed to the value

#90071 - $15.00 USD Received 27 Nov 2007; revised 4 Jan 2008; accepted 4 Jan 2008; published 9 Jan 2008
(C) 2008 OSA

obtained by the refractive index profile analysis [10]. The theoretical curve in Fig. 4 describes the data (open circles) reasonably well.

Table 1. Model parameters of Eq. (12), which correspond best to the experimental data shown in Fig. 4 obtained by a least-square theoretical analysis.

$\Delta d_{\max}/d_{\text{bulk}}$	$G_{el,0}$ [10^{22}eV/cm^3]	γ_{el}	μ
-1	41 ± 5	1.66 ± 0.3	1.07

5. Electro-optic modulation

A first electro-optic modulation in the produced ion implanted planar waveguide structures was demonstrated with the experimental configuration shown in Fig. 5. The laser output at a wavelength of $1.55\,\mu$m was coupled into the waveguides by conventional end-fire coupling. The propagation direction of the guided light was along the dielectric x_2 direction and its polarization was parallel to x_1.

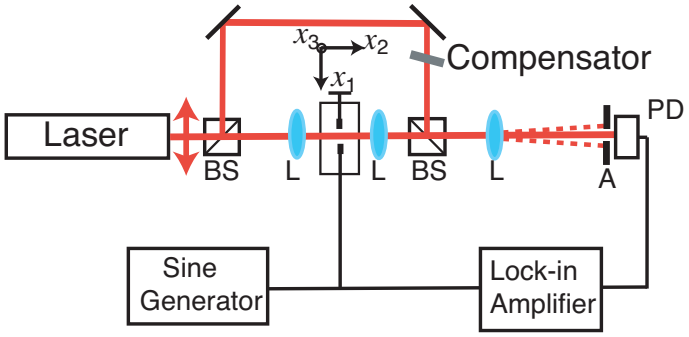

Fig. 5. Experimental setup with reference arm for electro-optic modulation. BS: beamsplitter, L: lens, A: aperture, PD: photodiode.

To detect the phase modulation of the guided signal, an external reference arm was set up. The resulting interference pattern was widened up with a lens and the central part of one fringe was selected with an aperture, which was placed in front of the photodiode.

The spacing between the gold electrodes with a thickness of about 70 nm was relatively large ($D = 2$ mm). To maximize the modulator response, the phase shift between the two arms was adjusted using a compensator. The resulting linear amplitude modulation was measured with a lock-in amplifier. From the modulation depth the electro-optic coefficient was determined with help of the following equations. The induced phase shift $\Delta\varphi$ is related to the electro-optic coefficient r_{111} for an electric field applied along the x_1 direction by [18]

$$\Delta\varphi = \frac{\pi r_{111} n_1^3}{\lambda} \frac{L_o}{D} U, \tag{13}$$

where n_1 is the refractive index, L_o the interaction length between the optical beam and the applied electric field and U the applied voltage to the electrodes. The interaction length was $L_o = 1.9$ mm and we applied sinusoidal modulation voltages with amplitudes of up to 10 V. The amplitude of the measured intensity modulation δI is related to the electro-optic coefficient by

#90071 - $15.00 USD Received 27 Nov 2007; revised 4 Jan 2008; accepted 4 Jan 2008; published 9 Jan 2008
(C) 2008 OSA

[18]

$$\delta I = \frac{I_{\max} - I_{\min}}{2} \frac{\pi r_{111} n_1^3}{\lambda} \frac{L_o}{D} \delta U, \tag{14}$$

where $I_{\max}$ and $I_{\min}$ are the maximal and minimal intensities measured by changing the optical length of the interference arm and δU is the amplitude of the applied modulation voltage. We obtained $r_{111} = 42 \pm 10$ pm/V at a modulation frequency of 2 kHz, which is about 10% lower compared to the bulk value of 47 ± 8 pm/V [7].

As for the nonlinear optical susceptibility, Eqs. (3) and (7), the electronic contribution to the electro-optic effect r^e can be written as [18]

$$r^e = 2N \frac{f_\omega^2 f_0}{n_\omega^4} \beta(-\omega, \omega, 0) \tag{15}$$

for the bulk and

$$\tilde{r}^e(z) \approx 2N p(z) \frac{\tilde{f}_\omega^2(z) \tilde{f}_0(z)}{\tilde{n}_\omega^4(z)} \beta(-\omega, \omega, 0) \tag{16}$$

for the implanted material, where $f_0 = (\varepsilon + 2)/3$. Their ratio is given by

$$\frac{\tilde{r}^e(z)}{r^e} = p(z) \frac{\tilde{f}_\omega^2(z) \tilde{f}_0(z)}{f_\omega^2 f_0} \frac{n_\omega^4}{\tilde{n}_\omega^4(z)}. \tag{17}$$

At the position of the maximal optical field of the first mode ($z = 2.7\,\mu$m), see Fig. 1, the electro-optic coefficient is only reduced by 2%, considering the parameters obtained in Section 4, and assuming that the reduction in ε is the same as for $n^2_{\omega\to 0}$. At the barrier position the electronic contribution to the electro-optic coefficient is reduced by 7%. Therefore, the measured reduction of the electro-optic coefficient agrees within the error well with the modeled one.

In our case the length of the waveguide was similar to the distance between the electrodes, therefore the required voltage to achieve $\pi/2$ phase shift is approximately equal to the reduced half-wave voltage of $\lambda/n^3 r = 3.4$ kV at 1.55 μm, which is about 40% lower as in (bulk) $LiNbO_3$. For the target devices in DAST crystals with an electrode distance below 5 μm, the half-wave voltage-interaction length product will be below 1.7 volt-centimeters.

6. Conclusions

We have determined the nonlinear optical properties of ion implanted waveguides in the organic crystal DAST by reflection second-harmonic generation measured from a wedged-polished sample. The planar waveguide structures investigated have been produced by H^+ ion implantation with a fluence of 1.25×10^{14} ions/cm^2. The measurements showed that the nonlinear optical susceptibility is preserved to more than 90% of the bulk value in the waveguide core region. A model that relates the microscopic material changes with the measured macroscopic properties has been introduced. The fraction of modified molecules after implantation has been determined with help of this model. In the barrier region less than 10% of the molecules are modified. In addition, a first electro-optic modulation in the planar waveguide structures has been demonstrated. We believe these results constitute an important step towards the utilization of organic nonlinear optical active crystals in integrated devices for telecommunication applications.

Acknowledgments

We thank J. Hajfler for his careful sample preparation and B. Ruiz, R. Gianotti and M. Sturzenegger for the crystal growth. This work has been supported by the Swiss National Science Foundation.

#90071 - $15.00 USD Received 27 Nov 2007; revised 4 Jan 2008; accepted 4 Jan 2008; published 9 Jan 2008

(C) 2008 OSA